DESIGN OF AN AXIAL FLUX BRUSHLESS DC MOTOR WITH CONCENTRATED WINDING FOR ELECTRICS VEHICLES

S. TOUNSI and R. NEJI

Ecole Nationale d'Ingénieurs de Sfax (ENIS)
Laboratoire d'Electronique et des Technologies de l'Information (LETI)
BP 1173 3038 Sfax TUNISIE
souhir.tounsi@isecs.rnu.tn ; rafik.neji@enis.rnu.tn

Abstract: *This paper describes a design methodology of an axial flux Brushless DC motor modular structure with concentrated winding, reducing the energy consumption of electric vehicles as well as their cost. This methodology rests on the development of an analytical dimensioning model of the motor - converter taking in account of several technological, physical constraints related to the global system. This model is validated as well as completed by finite elements simulations. The coupling of this model to the power train losses model and the motor mass model pose an optimization problem of the consumption and the cost of electrics vehicles. This problem is solved by the software optimization based on the Genetic Algorithms method described in [1].*

Key words: Electric vehicle, motor, converter, design, optimization.

1. Introduction

Currently and in look of the strong petroleum crises, during these last decades and the problems of atmospheric pollution, the electrification of vehicles project became a project of actuality. In this context, several works of research are thrown on this thematic [2], [3], and [4].

The electric vehicle production in big series is braked by their elevated cost as well as their weak autonomy. In this context, a modular axial motor structure and with permanent magnet reducing the cost of manufacture is chosen.

We choose the analytic method to conceive the whole motor converter seen its compatibility to optimization approaches. Indeed, it's fast and product results quickly and without iterations. The developed analytic model is validated by the finites elements method.

The coupling of power train losses model and the model of the motor mass to the program dimensioning the motor - converter, pose an optimization problem. This last is solved by the software of optimization based on the Genetic Algorithm method.

2. Control strategy

2.1 Electric vehicle power train structure

The synoptical schema of the electric vehicle power train is illustrated by figure1:

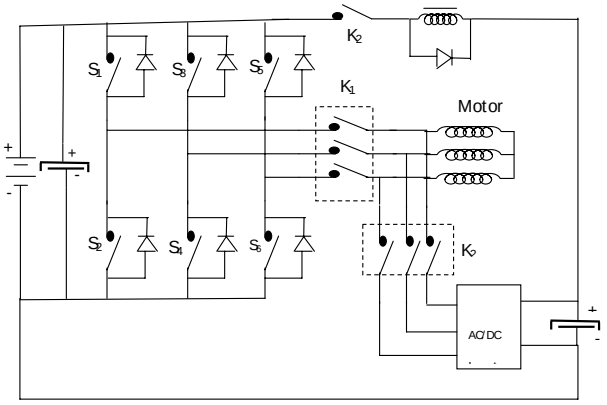

Fig. 1 . Electric vehicle power train structure

Figure 2 illustrates the PWM food principle of trapezoidal wave-form configuration

Naturally, DC/AC converter feeding the motor is with IGBTs allowing to an important energy losses [3], [1]. In our case, we have chosen a structure with electromagnetic switches leading to a reduction of the energy losses. The control of these switches is assured by six generating windings. Being fed by a sufficient current, these windings attract their ferro-magnetic cores, leading to the closings or the openings of these switches according to the control strategy maintaining the current in phase with the electromotive force. At the time of their dice-food these windings free the energy stocked through a free wheel diode. Two working phases are possible:

- Working in motor phase: in this phase the K_1 switches are closed and generating windings assures

the opening and the closing of the converter's switches according to a control strategy maintaining the current in phase with the electromotive force conducting to the reduction of the energy consumption. This phase is possible for working either in accelerated phase or in constant speed. During this phase the K_2 switches are open.

- Working in generating phase: this phase is possible for a working in decelerated phase. In this phase, the motor function in generator. The control system opens the switches of the static converter and the K_1 switches. At this moment the energy recuperation system functions. In this phase, the K_2 switches close itself to convert the three electromotive forces of the motor that absorbed itself according to the speed decreasing during the time on DC voltage. The recovered DC voltage is filtered by a capacitor. This voltage source is converted in a current source permitting the injection of electrons in the battery. This last is in charge thereafter. This phase is named: energy recuperation phase. The duration of this phase is until the stability of the speed or the acceleration of the vehicle.

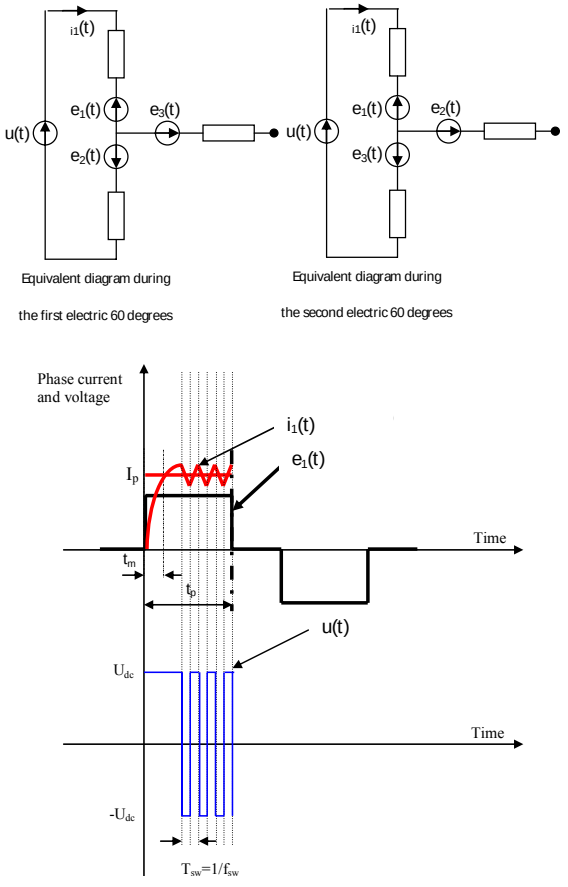

Fig . 2 . PWM food principle of trapezoidal wave-form configuration

2.2. Converter continuous voltage

The motor constant is defined by :

$$K_e = 2 \times n \times N_s \times A \times B \times B_g \quad (1)$$

For the axial flux structures A and B are given by:

$$A = \frac{D_e - D_i}{2} \quad (2)$$

$$B = \frac{D_e + D_i}{2} \quad (3)$$

Where D_e and D_i are respectively the external and the internal diameter of the axial flux motor, N_s is the number of spire per phase, n is the module number and B_g is the flux density in the air-gap.

The converter's continuous voltage U_{dc} is calculated so that the vehicle can function at a maximum and stabilized speed with a weak torque undulation. The electromagnetic torque that the motor must exert at this operation point, via the mechanical power transmission system T_{Udc} (reducing + differential) is estimated by the following expression:

$$T_{Udc} = \frac{P_f}{\Omega} + T_d + \left(T_b + T_{vb} + T_{fr}\right) + \frac{T_r + T_a + T_c}{r_d} \quad (4)$$

Where T_b is the rubbing torque of the motor, T_{vb} is the viscous rubbing torque of the motor, T_{fr} is the fluid rubbing torque of the motor, T_r is the torque due to the friction rolling resistance, T_a is the torque due to the aerodynamic force, T_c is the torque due to the climbing resistance, T_d is the reducer losses torque and P_f are the iron losses and Ω is the motor angular speed.

At this operation point, the phase current is given by the following relation:

$$I_p = \frac{T_{Udc}}{K_e} \quad (5)$$

The only possibility making it possible to reach the current value I_p with a reduced undulation factor (10% for example) is to choose the converter's continuous voltage solution of the following equation [6]:

$$r = \frac{t_m}{t_p} = 10\% \quad (6)$$

Where t_p is the phase current maintains time at vehicle maximum speed and t_m is the boarding time of the phase current from zero to I_p [6]:

$$t_m = -\frac{L}{R} \times \ln\left(1 - \frac{2 \times R \times I_p}{U_{dc} - K_e \times \Omega_{max}}\right) \quad (7)$$

Where R and L are respectively the phase resistance and inductance and Ω_{max} is the maximum angular velocity of the motor.

The phase current maintains time at maximum speed of vehicle (corresponds to 120 electric degrees) is given by the following formula [6]:

$$t_p = \frac{1}{3} \times \frac{2 \times \pi}{p \times \Omega_{max}} \quad (8)$$

The converter's continuous voltage takes the following form:

$$U_{dc} = \frac{2 \times R \times I_p}{1 - \exp\left(- \frac{2 \times \pi \times r}{3 \times p \times \Omega_{max} \times \frac{L}{R}} \right)} + K_e \times \Omega_{max} \quad (9)$$

The phase inductance of the all configurations is expressed as follows [6]:

$$L = \frac{3 \times \mu_0}{N_t} \times \left(\frac{A_t}{g + t_m} + \frac{A \times h_s}{2 \times A_s} \right) \times N_s^2 \quad (10)$$

Where μ_0 is the air permeability, A_t is slot area, t_m is the magnet thickness, h_s is slot height, g is the air-gap thickness and A_s is the slot width.

The converter continuous voltage increases by increasing of the vehicle speed which validates the fact of calculating its value at maximum speed. Two important factors involving the increase of the converter continuous voltage:

- The increase of the motor electric constant.
- The reduction of the undulation factor.

Consequently, a compromise between the reduction of the converter continuous voltage directly related to the space reserved for the battery and the reduction of undulation factor is to be found.

2.3 Design of generating winding

The generating windings assure the closing and the opening of DC/AC converter electromagnetic switches, according to the chosen of control law. When a winding is fed by a sufficient current, it attracts its core and drags the closing of one or switches attached to its Ferro-magnetic core thereafter. The current feeding this windings, must be sufficient to defeat the opposite strength generated by the recall spring.

The structure of the generating winding is illustrated by the following face:

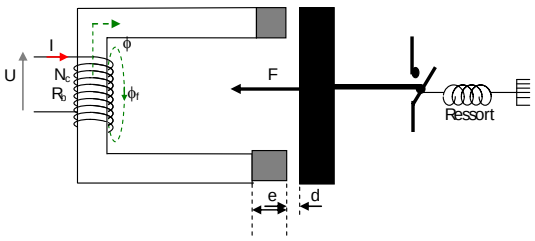

Fig. 3 . Generating winding

The generating winding inductance depends on the displacement of the mobile iron core:

$$L_b = \frac{N_c^2}{\Re_t} = \frac{N_c^2}{\frac{2 \times e}{\mu_0 \times S} + \frac{2 \times (d - x)}{\mu_0 \times S}} = \frac{\mu_0 \times S \times N_c^2}{2 \times (e + d - x)} \quad (11)$$

Where N_c is the spires number of winding, μ_0 is the air permeability, S is the section of the iron core, x is the displacement of the iron core.

The energy stocked in the winding is given by the following equation:

$$W = \frac{1}{2} \times L_b \times I^2 \quad (12)$$

The power drifting of this energy is given by the following equation:

$$P = \frac{dW}{dt} = \frac{I^2 \times \mu_0 \times S \times N_c^2}{4} \times \frac{d}{dt} \left(\frac{1}{e + d - x} \right) \quad (13)$$

This electric power turns into a mechanical power to the level of the mobile iron core:

$$P = F \times V \quad (14)$$

Where F and V are respectively the attraction strength and the speed of the mobile iron core.

We deduct from the two equations (13) and (14) the expression of the attraction strength depending on the displacement x:

$$F = \frac{\mu_0 \times U^2 \times S \times N_c^2}{R_b^2} \times \frac{d}{dx} \left(\frac{1}{e + d - x} \right) = \frac{\mu_0 \times U^2 \times S \times N_c^2}{R_b^2} \times \left(\frac{1}{(e + d - x)^2} \right) \quad (15)$$

Where R_b, U and I are respectively the generating winding resistance, voltage and current. The equation that describes the working of the mobile iron core and switch, drift of the dynamics fundamental relation:

$$M_n \times \frac{dV}{dt} = F - m \times K \times x \quad (16)$$

Where M_n is the mass of the mobile iron core, K is recall spring constant and m is the number of attracted switches.

While replacing F by its expression, (15) becomes:

$$M_n \times \frac{dV}{dt} = \frac{\mu_0 \times U^2 \times S \times N_c^2}{R_b^2} \times \left(\frac{1}{(e+d-x)^2} \right) \quad (17)$$

$$- m \times K \times x$$

At the balance we have:

V = 0 et d = x, from where we deduct the expression of the food voltage:

$$U = \sqrt{\frac{4 \times m \times K \times e^2 \times R_b^2}{\mu_0 \times S \times N_c^2}} \quad (18)$$

The active section of the copper depends on the admissible current density in the copper δ:

$$S_c = \frac{I}{\delta} = \frac{U}{R_b \times \delta} \quad (19)$$

From the equations (17) and (18) we deduct the expression of the active section of winding copper thread:

$$S_c = \sqrt{\frac{4 \times m \times K \times e^2}{\mu_0 \times \delta^2 \times S \times N_c^2}} \quad (20)$$

The generating winding resistance is given by the following equation:

$$R_b = \frac{\rho \times L_e}{S_c} \quad (21)$$

Where ρ is the copper resistivity and L_e is the winding length:

$$L_e = 2 \times N_{c/c} \sum_{n=1}^{N_{cc}} \left(a + b + 2 \times n \times \sqrt{\frac{S_c}{\pi}} \right) \quad (22)$$

Where N_c is the total number of winding spires, $N_{c/c}$ is the number of thread layer rolled up, a and b are respectively the iron core width and thickness.

$$N_{c/c} = \frac{E_B}{2 \times \sqrt{\frac{S_c}{\pi}}} \quad (23)$$

Where E_B is the thickness of the copper thread rolled up.

The number of thread by layer is given by the following equation:

$$N_{cc} = \frac{N_c}{N_{c/c}} \quad (24)$$

From where the winding resistance is deduced by the following equation:

$$R_b = \frac{\rho \times \left(2 \times N_{c/c} \sum_{n=1}^{N_{cc}} \left(a + b + 2 \times n \times \sqrt{\frac{\sqrt{\frac{4 \times m \times K \times e^2}{\mu_0 \times \delta^2 \times S \times N_c^2}}}{\pi}} \right) \right)}{\sqrt{\frac{4 \times m \times K \times e^2}{\mu_0 \times \delta^2 \times S \times N_c^2}}} \quad (25)$$

3. Studied structures of the traction motor

3.1. Manufacturing cost reduction

The motor structure is modular i.e. it can be with several stages. This technology allows the reduction of the production cost of these motor types. The slots are right and open what facilitates the coils insertion and reduces the motor manufacturing cost. The concentrated winding is used because of its advantages:

- Reduction of the manufacturing time of this motor (insertion of coils in one block).
- Reduction of the end-windings.
- Reduction of the motor bulk.

Figure5 illustrates the first trapezoidal configuration (n=1) with axial flux only one stage [5].

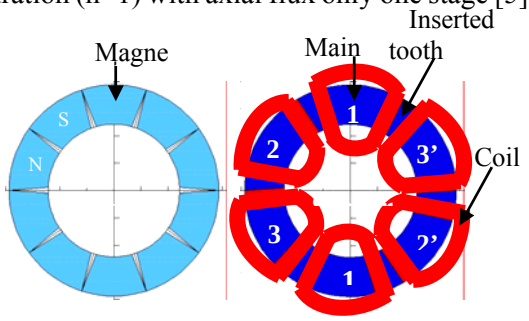

2-D schema of axial motor

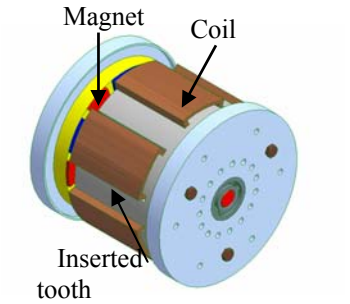

3-D schema of axial motor

Fig . 4 . 5 pairs of poles, 6 main teeth, axial flux and trapezoidal configuration

Five configurations with a trapezoidal wave-form are found while being based on optimization rules of the ripple torque and cost. Each configuration is characterized by a variation law of the pole pairs number (p) according to an integer number n varying from one to infinity, the ratio (r) of the number of main teeth (N_t) by the number of pole pairs, the ratio (ν) between the angular width between two main teeth and that of a principal tooth, the ratio (α) between the angular width of a principal tooth and that of a magnet and the ratio (β) between the angular width of a magnet and the polar step. Table .1 gives these ratios for these configurations [1].

Trapezoidal configurations	p	r	ν	α	β
1	2.n	1.5	1/3	1	1
2	5.n	1.2	2/3	1	1
3	7.n	6/7	4/3	1	1
4	4.n	0.75	5/3	1	1
5	5.n	0.6	7/3	1	1

Table 1: Found configurations

3.2. Design methodology

We choose the analytic modelling of the motor, because it's compatible to the optimisations approaches [1]. The analytic sizing step is inverted starting from needs (torque, motor velocity) towards geometry dimensions. While, in classical analytic sizing, the computation starts from geometry towards needs. Indeed the limit of the plan torque/velocity of the motor is given. The electrical motor has to be able to function in this plan without constraints. Here, the problem resolution is completely reversed. For example, the operating temperature is fixed and then computed. It should be also recognised that the inversion of the problem facilitates its resolution. In the same way, the designer fixes the induction. The worksheet includes 200 items of computed elements. The difficulty is to classify these elements and to distinguish results from data.

The worksheet computes the geometrical dimensions of rotor and stator as well as windings, temperature, inductance, leakages and efficiency for different operating points and control modes.

A sizing program is developed with equations detailed below. The program inputs are:

1. Electric vehicle specifications.
2. Materials properties.
3. Configuration, i.e. magnet number and teeth number.
4. Inner and outer diameter of the motor.
5. Notebook data.
6. Current density in coils δ.
7. Rotor yoke B_{ry}, stator yoke B_{sy}, flux density in the air-gap B_g, reducer ratio and number of spire per phase N_s.

When inputs 3. and 4. are set, magnet shapes, teeth and slots are fixed. Then, the area of one tooth A_t and the average length of a spire L_{sp} are calculated from geometric equations.

This model is validated by finite elements method. Indeed, the motor is drawn according to its geometrical magnitudes extracted from analytical model with the software Maxwell-2d, and is simulated in dynamic and static in order to compare the results obtained with those that are found by the analytical method.

The coupling of this model to a model evaluating the power train losses and motor mass, poses an optimization problem with several variables and constraints. This latter is solved by the genetic algorithms (GAs) method [1].

3.3. Dimensioning torque

The back electromotive force (E.m.f) stage level is given by the following expression :

$$E = n \times N_s \times A \times B \times \Omega \times B_g \quad (26)$$

The instantaneous electromagnetic power $P_e(t)$ is expressed by the following relation

$$P_e(t) = \sum_{i=1}^{m} e_i(t) \times i_i(t) \quad (27)$$

Where $e_i(t)$ and $i_i(t)$ are respectively the back electromotive force and the current of the phase i.

Two phases are fed simultaneously and the currents of phases have the same wave-form as the electromotive force with a maximum value of motor phase current I. Consequently, for a constant speed, the electromagnetic power developed by the motor takes the following form:

$$P_e = 2 \times E \times I \quad (28)$$

The electromagnetic torque developed by the motor is expressed by:

$$T_m = 2 \times \frac{E \times I}{\Omega} \quad (29)$$

The electromagnetic torque developed by the motor results:

$$T_m = 2 \times n \times N_s \times A \times B \times B_g \times I \quad (30)$$

The electromagnetic torque which the motor must develop so that the vehicle can move with a speed v is deduced from the dynamics fundamental relation related to the electric vehicle dynamic:

$$T_m = \frac{P_f}{\Omega} + T_d + \left(T_b + T_{vb} + T_{fr}\right) + \frac{T_r + T_a + T_c}{r_d} + \left(\frac{J}{R_w} + \frac{M_v \times R_w}{r_d}\right) \times \frac{dv}{dt} \quad (31)$$

Where r_d is the reduction ratio, M_v is the vehicle mass, R_w is the vehicle wheel radius, J is the motor moment of inertia and v is the vehicle velocity.

The different torques are expressed by the following equations [6]:

$$T_b = s \times \frac{v}{|v|} \quad (32)$$

$$T_{vb} = \chi \times v \quad (33)$$

$$T_{fr} = k \times v \times |v| \quad (34)$$

$$T_r = R_w \times f_r \times M_v \times g \quad (35)$$

$$T_a = R_w \times \frac{(M_{va} \times C_x \times A_f)}{2} \times V^2 \quad (36)$$

$$T_c = M_v \times g \times \sin(\lambda) \quad (37)$$

Where s is the dry friction coefficient, χ is the viscous friction coefficient, k is the fluid friction coefficient, λ is the angle that the road makes with the horizontal, M_{va} is the density of the air, C_x is the aerodynamic drag coefficient, r_p is a coefficient taking account of the mechanical losses in the motor and the transmission system, and A_f is the vehicle frontal area. The phase current becomes:

$$I = \frac{T_m}{2 \times n \times N_s \times A \times B \times B_g} \quad (38)$$

The dimensioning current is expressed as following:

$$I_{dim} = \frac{T_{dim}}{2 \times n \times N_s \times A \times B \times B_g} \quad (39)$$

T_{dim} is the dimensioning torque. This torque is found by the genetic algorithm method on a standardized circulation mission in order to not exceed the limiting temperatures and to minimize the motor mass.

Several methods were proposed to define dimensioning sizes of the motor-reducer torque, based on simplified statistical tools [2], [4]. The first method is based on the determination of the effective torque for a circulation mission in order to take into account the thermal aspect [2], [4]. A second more elaborate approach consists in defining zones of strong occurrences and to take the sizes resulting from these zones like dimensioning sizes. Finally, a last simpler method consists in dividing the torque-speed plan into 4 zones, to take the gravity center of each zone then to consider the gravity center of these four points balanced by the number of each zone points as dimensioning point. These methods have the advantage of quickly providing useful sizes for dimensioning and simulation, nevertheless they do not take into account the problem of electric vehicle consumption minimization. For our approach, the dimensioning torque will be iteratively calculated by the genetic algorithms method in order to satisfy a global optimization of autonomy while respecting the dimensional thermal stresses relating to our application specified by the schedule of conditions. To guide the algorithm to converge towards a powerful solution and in order to limit the space of research, the motor dimensioning torque must satisfy the following condition extracted inequality:

$$(1-\varepsilon) \times R_w \times \left(\frac{\frac{J}{R_w^2} + \frac{M_v}{r_d}}{t_d} \times V_b + \frac{M_v \times g \times \sin(\lambda)}{r_d}\right) \leq T_{dim} \leq (1+\varepsilon) \times R_w \times \left(\frac{\frac{J}{R_w^2} + \frac{M_v}{r_d}}{t_d} \times V_b + \frac{M_v \times g \times \sin(\lambda)}{r_d}\right) \quad (40)$$

The adjustment coefficient of the torque ε generally does not exceed 0.25 and will be adjusted by simulations of the propulsion system on normalized circulation missions.

Figure 5 illustrates the evolution of motor torque in versus vehicle speed for a reducing ratio equal to 3.

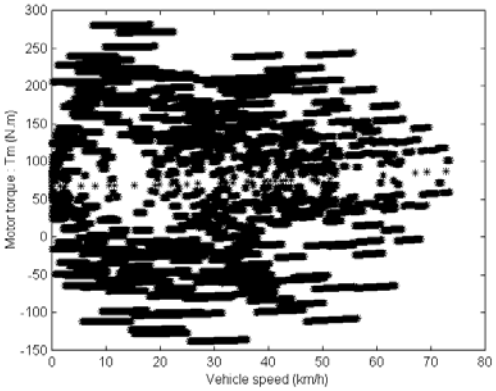

Fig. 5 . Motor torque evolution in versus electric vehicle speed

This figure shows that the dimensioning torque is around 250 Nm, which validates inequality (40).

3.4. Motor sizing

The air-gap flux density is calculated for a maximal recovery position, or the magnet is in front of a main tooth. At this position the air-gap flux density is maximal. The distribution of the field lines to the level of a pole is illustrated by the following face:

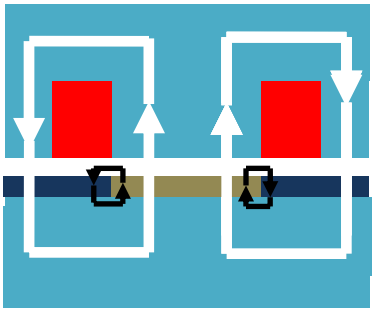

Fig. 6 . Flux lines distribution at maximal recovery position

The flux decomposes itself in main flux assuring the traction of the rotor by interaction with the stator flux and in leakages flux between magnets.

As applying the Ampere theorem to the level of a stator pole, we can deduct the flux density due to the food of a stator coil.

$$\int_{\text{flux lines}} \vec{H}\times\vec{dl}=\frac{N_s}{2}\times I_{max}=2\times\left(H_{ri}\times t_m+H_{ri}\times g\right) \quad (41)$$

Where I_{max} is the maximal current feeding the motor, H is the magnetic field, H_{ri} is the air-gap magnetic field, t_m is the magnet thickness and μ_0 is the air permeability.

$$B_{ri}=\mu_0\times H_{ri} \quad (42)$$

Where B_{ri} is the flux density in the air-gap due to the food of stator coil.

$$Bri=\frac{\mu_0}{4}\times\frac{N_s\times I_{max}}{t_m+g} \quad (43)$$

While applying the Ampere theorem, we can deduct the magnet thickness imposing a fixed flux density in the different zones of the motor while disregarding the flux density due to the food of the stator coils, since the flux must cross two times the air-gap thickness and magnet with permeability very close to the air permeability.

$$\int_{\text{flux lines}} \vec{H}\times\vec{dl}=0=2\times\left(H_m\times t_m+H_g\times g\right) \quad (44)$$

The air-gap flux density is linear according to the magnetic field for this working regime:

$$B_g=\mu_0\times H_g \quad (45)$$

While applying the flux conservation theorem to the level of the air-gap, we deduct the value of the air-gap flux density in function of the magnet flux density and the coefficient of the leakages flux.

$$B_m\times S_m\times K_{fu}=B_g\times S_m \quad (46)$$

The magnet flux density becomes:

$$B_m=\frac{B_g}{K_{fu}} \quad (47)$$

The magnet flux density is approached by the following linear equation:

$$B_m=\mu_0\times\mu_m\times H_m+B_r \quad (48)$$

Where μ_m is the magnet's relative permeability, B_r is the remanence.

From the equation (44), (45), (46) and (48), we deduct the magnet thickness fixing the air-gap flux density equal to B_g,:

$$t_m=\mu_m\times\frac{B_g}{B_r-\frac{B_g}{K_{fu}}}\times g \quad (49)$$

Where $K_{fu} < 1$ is the magnet's leakage coefficient and g is the air-gap thickness. To avoid demagnetization, the phase currents must be lower hen the demagnetization current I_d [7]:

$$I_d=\left(\frac{B_r-B_{min}}{\mu_m}\times t_m-B_{min}\times K_{fu}\times g\right)\times\frac{p}{2\times\mu_0\times N_s} \quad (50)$$

Where B_{min} is the minimum flux density allowed in the magnets and μ_0 is the air permeability. The rotor yoke thickness t_{ry} and stator yoke thickness t_{sy} derive from the flux conservation [8]:

$$t_{ry}=\frac{B_g}{B_{ry}}\times\frac{Min\left(A_t,A_m\right)}{2\times A}\times\frac{1}{K_{fu}} \quad (51)$$

$$t_{sy}=\frac{B_g}{B_{sy}}\times\frac{Min\left(A_t,A_m\right)}{2\times A} \quad (52)$$

Where A_t is the tooth area, A_m is the area of one magnet, B_{ry} and B_{sy} are respectively the flux densities in rotor and stator yokes. For the axial flux and trapezoidal wave-form motor configurations the slot height is [7]:

$$h_s=\frac{3\times 2\times N_s}{2\times N_t}\times\frac{I_{dim}}{\delta}\times\frac{1}{K_f}\times\frac{1}{A_s} \quad (53)$$

Where N_t is the number of principal teeth, δ is the current density in slots, K_f is the slot filling factor, A_s is the slot width and I_{dim} is the dimensioning current:

$$I_{dim} = \frac{T_{dim}}{K_e} \quad (54)$$

The slot width is expressed as follows [13]:

$$A_s = B \times SIN\left(\frac{1}{2} \times \left(\frac{2 \times \pi}{N_t} - \alpha \times \beta \times \frac{\pi}{p} \times (1 - r_{did})\right)\right) \quad (55)$$

Where r_{did} is the ratio between the angular width of the inserted tooth and that of the principal tooth. This ratio is optimised by finite elements simulations in order to reduce the flux leakages and to improve the back E.m.f. wave-form.

3.5. Thermal model of the motor

A thermal nodal model of the electric motor is developed to respect thermals constraints [4]. This thermal model of the motor modular structure is developed while considering that the flux of heat propagates itself axially [8]. The following face illustrates this property:

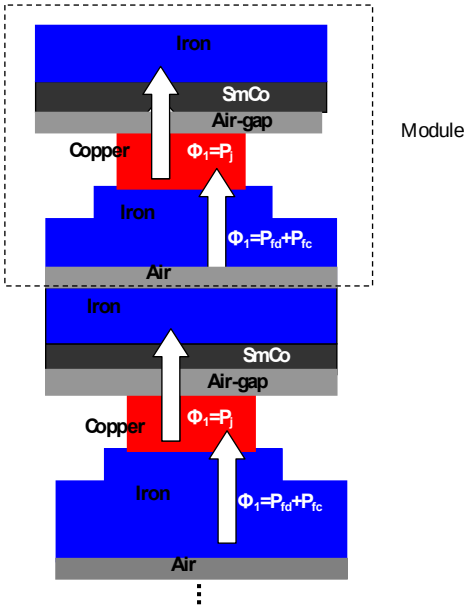

Fig. 7 . Thermal flux propagation

The nodal model of the motor structure is illustrated by the following figure:

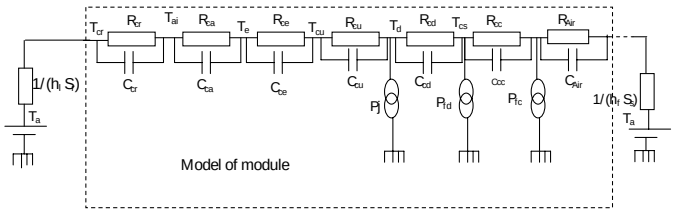

Fig. 8 . Thermal model of the motor structure

h_l	Free convection coefficient
S_r	Active section of the rotor
h_f	Forced convection coefficient
S_s	Active section of the stator
R_{cr}	Rotor yoke conduction resistance
R_c	Magnets conduction resistance
R_{ce}	Air-gap conduction resistance
R_{cu}	Copper conduction resistance
R_{cd}	Teeth conduction resistance
R_{cc}	Stator yoke conduction resistance
R_{Air}	Air conduction resistance
P_j	Copper losses
P_{fd}	Teeth iron losses
P_{fc}	Stator yoke iron losses
T_a	Ambient temperature
T_{cr}	Rotor yoke temperature
T_{ai}	Magnets temperature
T_e	Air-gap temperature
T_{cu}	Copper temperature
T_d	Teeth temperature
T_{cs}	Stator yoke temperature
C_{cr}	Capacity of rotor-Air, rotor-magnets contacts
C_{ca}	Capacity of magnets-rotor, magnets-airgap contacts
C_{ce}	Capacity of airgap-magnets, airgap-copper contacts
C_{cu}	Capacity of copper-airgap, copper-teeth contacts
C_{cd}	Capacity of teeth-copper, teeth-stator yoke contacts
C_{cc}	Capacity of stator-teeth, stator-air contacts
C_{AIR}	Capacity of air-stator, air cooling system contacts

Table 2: Nomenclature of the nodal model diagram

4. Complementarity and validation study of the analytical model

Modelling by finite elements is a study of adjustment and also a stage of validation. The finite elements analysis of the axial flux synchronous motors is naturally a three-dimensional problem but a transformation is applied to have a two-dimensional model of which the use is more malleable and also faster. A parameterized model including many parameters is then developed.

4.1 Cylindrical cut plan transformation

The engine can be studied in 2D by decomposition in cylindrical plans of cuts which produce different models. This choice is made in order to reduce the time of simulation. The variation of surface in glance enters a magnet and a principal tooth is not perfectly linear because of the principal edges. To find the true variation of flux, it is necessary to study the motor on several plans of cylindrical cuts. But it was shown that non-linearity coming from the variation of surface in glance enters a magnet and a principal tooth is very low for the structure.

Another simplification consisting in supposing that the magnetic material is linear was validated.

In conclusion, the motor is studied on an average contour with simulations into linear.

Figure 9 shows the finite elements model of the selected configuration

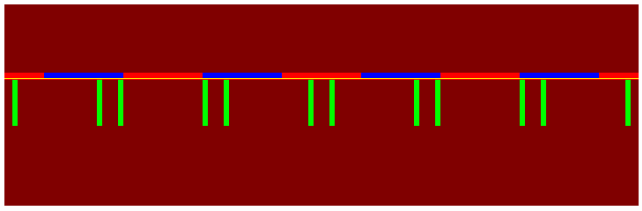

Fig. 9 . Cylindrical cut plan model of the selected configuration

4.2. Axial/radial transformation

The motor with axial flux is studied by its equivalent with radial flux. The transformation is carried out on an average contour of the engine with axial flux. To have the same back E.m.f., it is necessary that the average diameter of the axial structure is equal to the average diameter of the motor with radial flux ($D_m = (D_e+D_i)/2$), and the length of the radial motor Lm is equal to $(D_e-D_i)/2$ [2].

It should be noted that to have the same magnetic flux densities in the various zones of the two structures, it is necessary that these last have the same thickness of magnet, same thickness of stator and rotor yoke and the same height of teeth.

4.3 Finite elements model

The mesh of the air-gap is achieved in three layers. This increase of the number of nodes is necessary to have a good temporal representation. The finite elements problem is solved by using the Maxwell-2D program. The solver allows the use of external electric circuits.

The distribution of the flux lines when the motor operates at no-load is illustrated in figure 10.

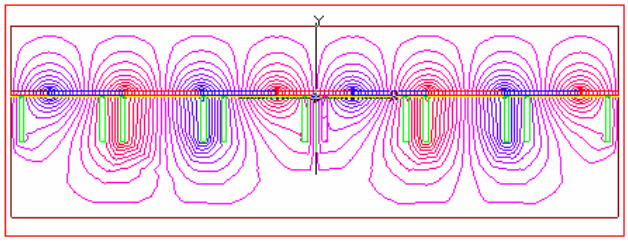

4 pairs of poles, 6 main teeth and axial trapezoidal wave-form structure

5 pairs of poles, 6 main teeth and radial trapezoidal wave-form structure

Fig. 10 . Filed lines at no-load

4.4. Simulation results

The flux at load and at no load calculated by finite elements analysis is illustrated by figure 11.

Flux reaches the maximum value calculated by the analytical method what validates this approach. Flux is perfectly linear, which leads to obtaining perfectly trapezoidal back E.m.f. (figure 12). This motor property reduces considerably the torque undulations.

The electromagnetic torque is calculated by this equation:

$$T_m(t) = \frac{1}{\Omega} \times \sum_{i=1}^{3} E.m.f._i(t) \times i_i(t) \qquad (56)$$

The torque value achieves its value calculated by analytical model which validates entirely this dimensioning method.

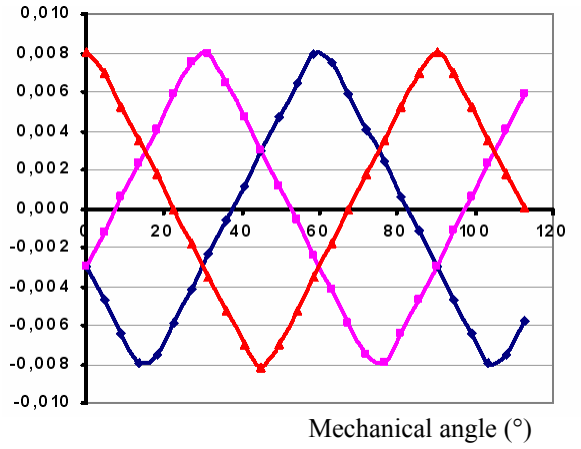

Flux at no load

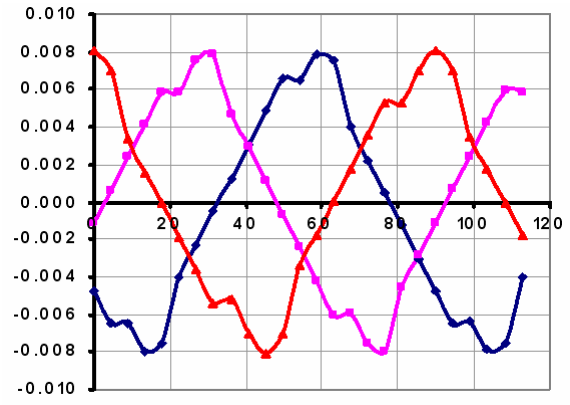

Flux at load

Fig. 11 . Three phases flux

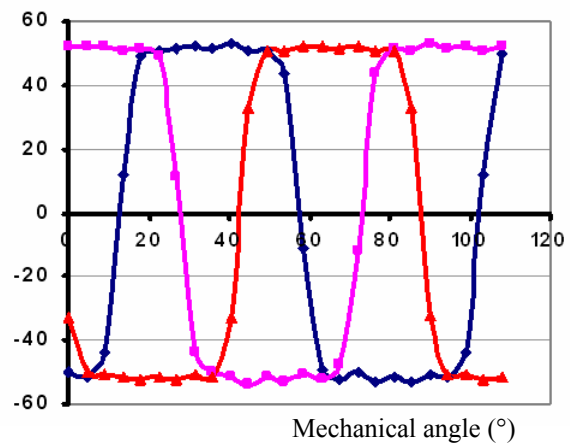

E.m.f. at no load

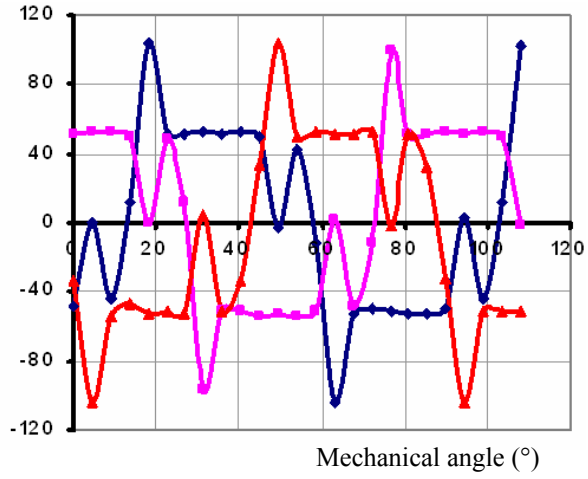

E.m.f at load

Fig. 12 . Three phases E.m.f.

4.5 How to compute the inductance

The inductance value is usually low for this type of machine because the flux created by the coil must cross the air-gap and the magnet thickness. In order to compute the inductance, the motor is supplied by its peak current and the magnets are replaced by air [5]. The flux lines distribution around one stator pole are illustrated by figure 13.

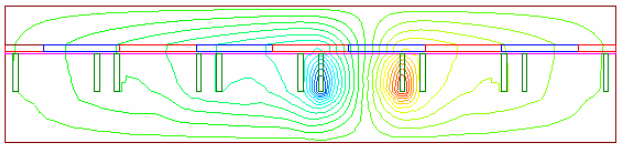

Fig. 13 . Flux lines distribution around one stator pole

The motor air-gap is relatively large producing then important flux leakages in slots. For a linear system, the inductance value of a phase constituted by two coils may be obtained from:

- The energy calculation:

$$L = \frac{2}{I^2} \times A \times \iint_{area} B_m \times H \times ds \quad (57)$$

- The flux calculation:

$$L = \frac{N_s}{I} \times \frac{1}{s_{slot}} \times A \times \int A_s \cdot ds \quad (58)$$

Where B_m is the flux density, H is the magnetic field, s is the slot area and A_s is scalar potential.
The finite elements analysis valid the analytic model of inductance.

5. Optimisation problem

5.1. Modelling of motor mass and power train losses

The motor weight is expressed as following:

$$W_m = W_{sy} + W_t + W_c + W_{ry} + W_m \quad (59)$$

For the axial flux configurations the weight of stator yoke W_{sy}, tooth W_t, copper W_c, rotor yoke W_{ry}, and magnets W_m are expressed as following:

$$W_{sy} = n \times d \frac{\pi}{4} \times \left(D_e^2 - D_i^2\right) \times t_{sy} \quad (60)$$

$$W_t = n \times d \times N_t \times A_t \times h_s \quad (61)$$

$$W_c = 3 \times n \times N_s \times L_{sp} \times \frac{I_{dim}}{\delta} \times d_c \quad (62)$$

$$W_{ry} = \pi \times \left(\left(\frac{D_e}{2}\right)^2 - \left(\frac{D_i}{2 \times 1}\right)^2 \right) \times t_{ry} \times d \quad (63)$$

$$W_m = 2 \times n \times p \times A_m \times t_m \times d_m \quad (64)$$

Where d is the density of the metal sheet, d_c is the density of copper, d_m is the magnet density, A_a is the magnet angular width, A_d is the angular width of principal teeth and A_e is the slot angular width.

Several modeling types of the electric vehicles power train integrating to energy losses optimization approaches exist. We mention for example, the model of the power train implanted under the environment of finite element field calculation software [9], and the model describing the electric behavior of the power train based on the choice of a control law [10], [14].

The resolution of an optimization problem with several variables and constraints by the first method is very heavy, since the resolution of problems by the finite element method requires an important time [5], what limits the performance of its integration to optimization approaches. The second method is as heavy, since it reproduces the electric behavior of the power train according to a control law imposing a very weak calculation step. This last is essentially bound to the switched frequency, especially to big speed. It also presents the inconvenience of the possibility to diverge, since the parameters of the regulators are also fixes, and the evolution of the optimization parameters is iterative. It can provoke problems of compatibility thereafter between the control law and the design approach [11].

In our case, our choice is carried on the inverse gait of modeling taking in account the hypothesis disregarding the current undulation due to the shape chopped of the the motor phase voltage. The currents waves shapes are supposed ideal and in phase with the electromotive forces. This approach permits the calculation of the motor torque that the motor must develop to follow a mission of circulation, from the equation (31). The current is calculated while dividing the motor torque by the electric constant of the motor, what permits the calculation of the copper and battery losses. This method of resolution produces results them very quickly, what increases the performance of its integration infinitely to a big dimension optimization approaches.

For the trapezoidal wave-form configurations, the copper losses are expressed by the following relation:

$$P_c = 2 \times R \times I^2 \quad (65)$$

The phase resistance is given by the following expression:

$$R = r_{cu}\left(T_b\right) \times \frac{N_s \times L_{sp}}{S_c} \quad (66)$$

Where r_{cu} is the copper receptivity, L_{sp} is the average length of spire, T_b is the copper temperature and S_c is the active section of one conductor:

$$S_c = \frac{I_{dim}}{\delta} \quad (67)$$

The iron losses are expressed by the following relation [1]:

$$P_{fer} = C \times f^{1.5} \times \left(n \times W_t \times B_g^2 + n \times W_{sy} \times B_{sy}^2\right) \quad (68)$$

Where c is the core loss, f is the motor feeding frequency, W_t is the teeth weight, W_{sy} is the stator yoke weight, B_g is the ai-rgap flux density and B_{sy} is the flux density in stator yoke. The mechanical losses are expressed by the following relation [7]:

$$P_m = \left(T_b + T_{vb} + T_{fr}\right) \times \Omega \quad (69)$$

Where Ω is the angular speed of the electric motor.

The losses in the static converter are nearly hopeless, they are not held in account in the model of power train losses calculation.

Since two phases are always feeding, the losses in the battery are expressed by the following expression:

$$P_b = 2 \times R_{batt} \times I_b^2 \quad (70)$$

Where R_{batt} is the internal resistance of the battery. The power train losses is expressed consequently by the next equation:

$$P_{ptl} = P_c + P_{fer} + P_m + P_b \quad (71)$$

The model of the power train losses is coupled to the electric vehicle power train model. This model is illustrated by the following face.

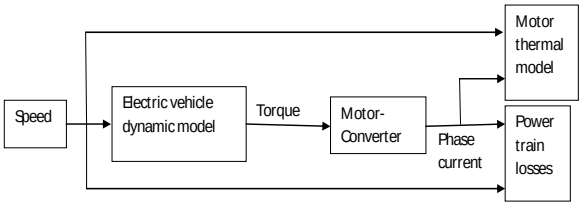

Fig. 14 . Electric vehicle power train model

5.2. Genetic algorithms optimization of the motor mass and the power train losses

The function to optimize is expressed by the following expression:

$$F_o = W_m + a\, P_{ptl} \quad (72)$$

Where "a" is a coefficient fixing the influence degree of P_{ptl} at the global objective function compared to W_m. Indeed, "a" brings closer the value of (a P_{ptl}) to the value of W_m.

The optimization problem consists in optimising the F_o with respect to the problem constraints. In fact, Genetic Algorithms (GAs) are used to find optimal values of the switched frequency f_{sw} , radius of the wheel in meters R_w, the gear ratio r_d, The adjustment coefficient of the torque ε, the internal diameter D_i, the external diameter D_e, the flux density in the air-gap B_g, the current density in the coils δ, the flux density in the rotor yoke B_{ry} , the flux density in the stator yoke B_{sy} and the number of phase spires N_s [12].

The beach of variation of each parameter xi $\in$ (f_{sw} , R_w, r_d, ε, D_i, D_e, B_g, δ, B_{ry} , B_{sy}, Ns) must respect the following constraint: $x_{imin} \leq x_i \leq x_{imax}$. The values of the lower limit x_{imin} and the upper limit x_{imax} are established following technological, physical and expert considerations, for example: The internal and the external diameter of the motor is delimited by the space reserved to the motor.

$$\left\{ \begin{array}{c} \text{maximise}\left(F_o\right) \\ \text{with :} \\ 500 \leq f_{sw} \leq 5000\ (\text{Hz}) \\ 0.25 \leq R_w \leq 0.35\ (\text{m}) \\ 1 \leq r_d \leq 8 \\ 0 \leq \varepsilon \leq 0.25 \\ 0.025 \leq D_i \leq 0.25\ (\text{m}) \\ 0.26 \leq D_e \leq 0.5\ (\text{m}) \\ 0.1 \leq B_g \leq 1.04\ (\text{T}) \\ 5 \leq \delta \leq 7\ (\text{A/mm}^2) \\ 0.1 \leq B_{ry} \leq 1.06\ (\text{T}) \\ 0.1 \leq B_{sy} \leq 1.6\ (\text{T}) \\ 10 \leq N_s \leq 1000 \\ r \leq 10\% \\ Udc \leq 100\ (\text{V}) \\ I \leq I_d\ (\text{A}) \\ T_a \leq 50\ (^\circ\text{C}) \\ T_b \leq 90\ (^\circ\text{C}) \end{array} \right. \quad (73)$$

Where T_a and T_b are respectively the magnets and the coils temperatures.

The genetic algorithms are an exploration algorithms resting on the natural selection and genetics mechanisms. They use an uncertain choice as tool to guide a highly intelligent exploration in the coded parameter space. They consist in making evolve a population of individuals with the help of the different operators: selection, crossing and mutation. The algorithm developed for the resolution is illustrated by the following figure [13]:

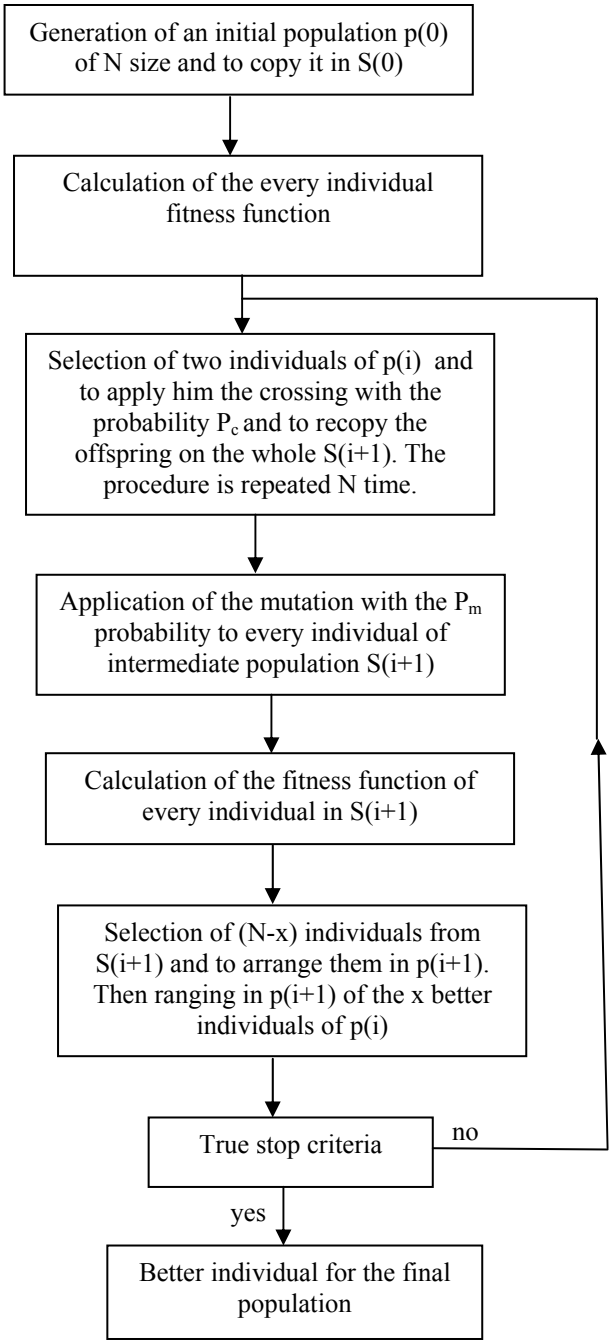

Fig. 15 . Optimization algorithm

This programs run at every iteration the simulation of the power train model to evaluate the fitness function. The particularity of this program is to allow at every iteration to a some number (x) of better individuals of population i to reproduce in population (i+1).

6. Conclusion

An analytical model dimensioning the whole motor converter is developed together with a validation and complementarity study by finite element method. This model is coupled to an optimization program in order to find the design and control parameters of the whole motor-converter minimizing the power train energy losses and the electric vehicle cost. This study aims to encourage the manufacture procedure of electric vehicles in big series [10].

References

[1] S.TOUNSI, R.NÉJI, F.SELLAMI : Conception d'un actionneur à aimants permanents pour véhicules électriques, Revue Internationale de Génie Électrique volume 9/6 2006 - pp.693-718

[2] Sid Ali. RANDI : Conception systématique de chaînes de traction synchrones pour véhicule électrique à large gamme de vitesse. Thèse de Doctorat 2003, Institut National Polytechnique de Toulouse, UMRCNRS N° 5828.

[3] C. C. Chan and K. T. Chau: "An Overview of power Electronics in Electric Vehicles", IEEE Trans. On Industrial Electronics, Vol, 44, No 1, February 1997, pp.3-13.

[4] C. PERTUZA : "Contribution à la définition de moteurs à aimants permanents pour un véhicule électrique routier". Thèse de docteur de l'Institut National Polytechnique de Toulouse, Février 1996.

[5] S. Tounsi, F. Gillon, S. Brisset, P. Brochet et R. NEJI: Design of an axial flux brushless DC motor for electric vehicle. ICEM2002 (15th International Conference on Electrical Machines), 26-28 August; Bruges-Belgium, CD: ICEM02-581.

[6] R. NEJI, S. TOUNSI, F. SELLAMI: Contribution to the definition of a permanent magnet motor with reduced production cost for the electrical vehicle propulsion. Journal European Transactions on Electrical Power (ETEP), Volume 16, issue 4, 2006, pp. 437-460.

[7] S. Tounsi, R. NEJI and F. SELLAMI: Mathematical model of the electric vehicle autonomy. ICEM2006 (16th International Conference on Electrical Machines), 2-5 September 2006 Chania-Greece, CD: PTM4-1.

[8] M. A. FAKHFAKH, M. HADJ KASEM, S. TOUNSI and R. NEJI: Thermal Analysis of Premanent Magnet synchronous Motor for Electric Vehicles. Journal of Asian Electric Vehicles, Volume 6, Number 2, December 2008.

[9] S. BRISSET, P. BROCHET: Shape Optimization of BDC Wheel Motor using Powell's Method. COMPEL vol. 19, no. 2, pp. 596-601, July 2000.

[10] B. Ben Salah, A. Moalla, S. Tounsi, R. Neji, F. Sellami: "Analytic design of Permanent Magnet Synchronous motor Dedicated to EV Traction with a Wide Range of Speed Operation", Internéational Review of Electrical Engineering (I.R.E.E), VOL 3, NO 1 January-February 2008"

[11] S. TOUNSI, N. BEN HADJ, R. NEJI and F. SELLAMI : Optimization of Electric Motor Design Parameters Maximising the Autonomy of Electric Vehicle. Internéational Review of Electrical Engineering (I.R.E.E), VOL 2, NO 1 January-February 2007"

[12] S. TOUNSI, R. NEJI and F. SELLAMI : Electric vehicle control maximizing the autonomy : 3rd International Conference on Systems, Signal & Devices (SSD'05), SSD-PES 102, 21-24 March 2005, Sousse, Tunisia.

[13] S. TOUNSI : Modélisation et optimization de la Motorisation et de l'Autonomie d'un véhicule électrique. Thèse de Doctorat 2006. Ecole Nationale d'Ingénieur de sfax-Tunisi.

[14] S.A. RANDI, S. ASTIER, B. SARENTI: Full Modeling Approach of Electric Vehicle for Design Optimisation. EVS 18 Berlin, 2001.